g-HDAF Multiresolution Deformable Models for Shape Modeling and Reconstruction *

I.A. Kakadiaris[1], M. Papadakis[2], L. Shen[1], D. Kouri[3], and D. Hoffman[4]
[1]Visual Computing Lab, Department of Computer Science,
Univ. of Houston, Houston, TX 77204-3010
[2]Department of Mathematics, Univ. of Houston, Houston, TX 77204
[3]Department of Physics, Univ. of Houston, Houston, TX 77204-5003
[4]Dept. of Chemistry and Ames Laboratory, Iowa State Univ., Ames, IS 50011

Abstract

In this paper, we construct a new class of deformable models using new biorthogonal wavelets, named Generalized Hermite Distributed Approximating Functional (g-HDAF) Wavelets. The scaling functions of this new family are symmetric and the corresponding wavelets optimize their smoothness for a given number of vanishing moments. In addition, we embed these multiresolution deformable models to the physics-based deformable model framework and use them for fitting 3D range data. We have performed a number of experiments with both synthetic and real data with very encouraging results.

1 Introduction

Modeling shapes is an integral part of computer vision driven by the need for shape reconstruction from sampled data and shape recognition. The deformable superquadrics introduced by Terzopoulos and Metaxas [13] represent the physics-based unification of the parameterized and the free-form modeling paradigms. The geometric structure of the models supports both global deformation parameters, which efficiently represent the gross shape features of an object, and local deformation parameters, which capture shape details. An important benefit of this global/local descriptive power in the context of computer vision is that it can potentially satisfy the often conflicting requirements of shape reconstruction and shape recognition. However, these models do not exhibit a smooth transition in the number of parameters required by the range of generated shapes.

To overcome this shortcoming, Vemuri and Radisavljevic [15] introduced a multiresolution hybrid modeling scheme that used an orthonormal wavelet basis [10]. By virtue of the multiresolution wavelet representation, their hybrid models have

*This work was supported in part by the following grants: NSF CAREER award CISE 9985482, NSF CHE-0074311, DMS-0070376, and R.A. Welch Foundation E-0608.

BMVC 2002 doi:10.5244/C.16.28

the unique property of being able to scale smoothly from global to local deformations depending on the number of the coefficients used to represent them. Thus, one may choose a set of wavelet coefficients at a particular decomposition level from the multiresolution representation of the hybrid model to augment the global parameters of the model.

In this paper, we construct a new class of multiresolution deformable superquadrics with respect to new biorthogonal wavelets, named Generalized Hermite Distributed Approximating Functional (g-HDAF) Wavelets. The scaling functions of this new family are symmetric and the corresponding wavelets exhibit enhanced smoothness for a given number of vanishing moments. In addition, we embed these multiresolution deformable models into the physics-based deformable model framework and use them for fitting 2D and 3D data. Our contributions are the following: 1) the development of a new class of linear phase wavelets (note that their associated scaling functions are symmetric with respect to the origin), 2) the development of a new class of deformable models using this new orthogonal wavelet basis, and 3) a comparative study of the wavelet transform of a deformable model's displacement map with respect to various commonly used orthonormal wavelets. The multiresolution wavelet basis that we have developed allows us to construct compact and diverse shape representations.

Our motivation to develop a new class of linear-phase wavelets stems from the fact that there are no known classes of well-localized (in the time domain) symmetric multiresolution filters. In fact, it is known that orthonormal compactly supported scaling functions cannot be symmetric (with the exception of the Haar scaling function) [2]. An important property of these newly developed g-HDAF wavelets is their enhanced smoothness as compared to the smoothness of the most commonly utilized classes of compactly supported orthonormal wavelets. This higher degree of smoothness together with their symmetry will increase the sparsity of the wavelet representation of the local deformations of the deformable models.

2 Methods

2.1 Biorthogonal g-HDAF wavelets

For the purposes of this paper, we construct a new class of Quadrature Mirror Filters (QMF) which we name *generalized HDAF biorthogonal filters*. Hermite Distributed Approximating Functionals (HDAFs) were introduced by Hoffman and Kouri in [4, 5]. Nonetheless HDAFs are not periodic functions so they are not QMFs [8]. Several classes of wavelets have been generated inspired by the original HDAFs with varying degrees of success (e.g., [6]).

Recently, we presented how to use HDAFs to construct low pass filters for orthonormal univariate scaling functions (which we dubbed *modified HDAF scaling functions*), which produced results that improved previous constructions [8]. An HDAF $h_{N,\sigma}$ is defined in the Fourier domain by:

$$\hat{h}_{N,\sigma}(\xi) = e^{-\frac{4\pi^2\xi^2\sigma^2}{2}} \sum_{n=0}^{N} \frac{\left(4\pi^2\xi^2\sigma^2\right)^n}{2^n n!} , \tag{1}$$

where $N \in \mathbb{Z}^+$ and $\sigma \in \mathbb{R}^+$. We modified the HDAF as follows [8]:

$$m_0(\xi) := \begin{cases} \hat{h}_{N,\sigma}(\xi) & \text{if} \quad |\xi| \leq \frac{1}{4} \\ \sqrt{1 - \hat{h}_{N,\sigma}(\xi - \frac{1}{2})^2} & \text{if} \quad \frac{1}{4} \leq \xi \leq \frac{1}{2} \\ \sqrt{1 - \hat{h}_{N,\sigma}(\xi + \frac{1}{2})^2} & \text{if} \quad -\frac{1}{2} \leq \xi \leq -\frac{1}{4} \end{cases},$$

and we extended m_0 1-periodically. We also imposed the condition $m_0(\frac{1}{4}) = \hat{h}_{N,\sigma}(\frac{1}{4}) = \frac{\sqrt{2}}{2}$. Then, $m_0(\xi)$ satisfied the orthogonality condition $|m_0(\xi)|^2 + \left|m_0(\xi + \frac{1}{2})\right|^2 = 1$, $\xi \in \mathbb{R}$, and $\hat{\phi}(\xi) := \prod_{j=1}^{\infty} m_0\left(\frac{\xi}{2^j}\right)$, $\xi \in \mathbb{R}$ is an orthogonal scaling function, which we called m-HDAF scaling function. For every N, the unique σ is determined by $\hat{h}_{N,\sigma}(\frac{1}{4}) = \frac{\sqrt{2}}{2}$.

In this paper, we introduce a new family of biorthogonal infinite impulse response (IIR) wavelet filters based on the HDAFs, which we name *generalized HDAF wavelets*. Recall that the auto-correlation of a function ϕ is defined by:

$$\Phi(x) = \int \phi(y)\phi(x - y)\, dy\ .$$

Clearly, $\widehat{\Phi}(\xi) = \widehat{\phi}^2(\xi)$, so $\widehat{\Phi}(2\xi) = m_0^2(\xi)\widehat{\Phi}(\xi)$. Since $\widehat{\Phi}$ is absolutely integrable and ϕ is in $L^2(\mathbb{R})$, one can assert that Φ can be replaced by a uniformly continuous function. With this remark in mind, we consider Φ to be uniformly continuous.

One can also verify that $\Phi(k) = \delta_{k,0}$, for all $k \in \mathbb{Z}$, and

$$M_0(\xi) + M_0(\xi + \frac{1}{2}) = 1, \tag{2}$$

where $M_0(\xi) = m_0^2(\xi)$. We refer to the filters that satisfy Eq. (2) as interpolating filters, and to such a Φ as an *interpolating scaling function*.

Proposition 1. *The following is true: $\Phi \in L^2(\mathbb{R})$, and the integer translates of $\Phi(x)$ form a Riesz basis of their closed linear span, i.e., there exist two constants $0 < c \leq C < \infty$, such that*

$$c \leq \sum_{k \in \mathbb{Z}} |\widehat{\Phi}(\xi + k)|^2 \leq C$$

where $c = e^{-\frac{\pi^4\sigma^4}{9}}$ and $C = 1$.

Proof: Since for all $\xi \in \mathbb{R}$, $\widehat{\Phi}(\xi) = \prod_{k=1}^{\infty} M_0(\frac{\xi}{2^k})$ and $M_0^2(\xi) + M_0^2(\xi + \frac{1}{2}) \leq [M_0(\xi) + M_0(\xi + \frac{1}{2})]^2 = 1$. A modification of the corresponding argument in [9] shows that $\Phi \in L^2(\mathbb{R})$.

Since $\sum_{k \in \mathbb{Z}} |\widehat{\phi}(\xi + k)|^2 = 1$, we have

$$\sum_{k \in \mathbb{Z}} |\widehat{\Phi}(\xi + k)|^2 = \sum_{k \in \mathbb{Z}} |\widehat{\phi}(\xi + k)|^4 \leq \sum_{k \in \mathbb{Z}} |\widehat{\phi}(\xi + k)|^2 = 1.$$

Since $|\widehat{\Phi}(\xi + k)|^2$ is an 1-periodic function, we can assume that $\xi \in [-\frac{1}{2}, \frac{1}{2}]$. Hence, $-\frac{1}{2} \leq \frac{\xi}{2^k} \leq \frac{1}{2}$ for every non-negative integer k. Therefore, $M_0(\frac{\xi}{2^k}) = \hat{h}_{N,\sigma}^2(\frac{\xi}{2^k})$.

Moreover,

$$\begin{aligned}\widehat{\Phi}(\xi) &= \prod_{k=1}^{\infty} e^{-(\frac{2\pi\xi\sigma}{2^k})^2}\left[\sum_{n=0}^{N}\frac{(\frac{2\pi\xi\sigma}{2^k})^{2n}}{2^n n!}\right]^2 \\ &= \left[\prod_{k=1}^{\infty} e^{-(\frac{2\pi\xi\sigma}{2^k})^2}\right]\left[\prod_{k=1}^{\infty}\sum_{n=0}^{N}\frac{(\frac{2\pi\xi\sigma}{2^k})^{2n}}{2^n n!}\right]^2 \\ &= e^{-\frac{4\pi^2\xi^2\sigma^2}{3}}\left[\prod_{k=1}^{\infty}\sum_{n=0}^{N}\frac{(\frac{2\pi\xi\sigma}{2^k})^{2n}}{2^n n!}\right]^2 \geq e^{-\frac{\pi^2\sigma^2}{3}}.\end{aligned}$$

This leads to $\sum_{k\in\mathbb{Z}}|\widehat{\Phi}(\xi+k)|^2 \geq \widehat{\Phi}^2(\xi) \geq e^{\frac{-2\pi^2\sigma^2}{3}}$. □

Proposition 1 implies that Φ is an interpolatory Riesz scaling function associated with an MRA. We say that a function $\mathcal{F}$ is stable, if $\mathcal{F}$ and its integer translates form a Riesz basis of their closed linear span.

To obtain a numerically stable decomposition and reconstruction algorithm, we need another function Φ^d. The integer translates of Φ and Φ^d must form a pair of dual Riesz bases. In other words, Φ and Φ^d must be stable and satisfy the following biorthogonal conditions:

$$\langle\Phi, \Phi^d(\cdot - k)\rangle = \delta_{k,0} \quad k \in \mathbb{Z}, \tag{3}$$

where $\langle\cdot,\cdot\rangle$ is the inner product of $L^2(\mathbb{R})$, and in this case Φ and Φ^d are dual functions. In the following, we present two different methods for constructing the dual scaling function Φ^d. The first method is used to construct Φ^d directly from Φ. The second method is used to design a dual filter M_0^d, and then construct Φ^d through the filter M_0^d. The filter M_0^d, which is a 1-periodic function, is a dual filter of a filter M_0, if

$$M_0(\xi)\overline{M_0^d(\xi)} + M_0(\xi+\frac{1}{2})\overline{M_0^d(\xi+\frac{1}{2})} = 1 \tag{4}$$

for all ξ in $[-\frac{1}{2}, \frac{1}{2}]$. Note that M may have more than one dual filters. It is well known that if Φ and Φ^d are stable and the corresponding lowpass filters satisfy Eq. (4), then they are dual functions. However, Eq. (4) is only a necessary condition for Φ and Φ^d to be a dual pair.

Method 1: The dual scaling function Φ^d can be defined as follows:

$$\widehat{\Phi}^d(\xi) = \frac{\widehat{\Phi}(\xi)}{\sum_{k\in\mathbb{Z}}|\widehat{\Phi}(\xi+k)|^2}.$$

Clearly, the functions Φ and Φ^d are biorthonormal, i.e., $\langle\Phi, \Phi^d(\cdot-k)\rangle = \delta_{k,0}$. Let c and C be the lower and the upper bound of the stable function Φ. Then Φ^d is also stable with lower bound C^{-1} and upper bound c^{-1}, respectively. This is due to the fact that $\sum_{k\in\mathbb{Z}}|\widehat{\Phi}(\xi+k)|^2$ is 1-periodic and $\sum_{k\in\mathbb{Z}}|\widehat{\Phi}^d(\xi+k)|^2 =$

$(\sum_{k\in\mathbb{Z}}|\widehat{\Phi}(\xi+k)|^2)^{-1}$. Thus, Φ and Φ^d is a pair of dual functions. The dual frequency response is given by:

$$M_0^d(\xi)=\frac{\widehat{\phi}^d(2\xi)}{\widehat{\phi}^d(\xi)}=\frac{M_0(\xi)}{M_0^2(\xi)+M_0^2(\xi+\frac{1}{2})}. \tag{5}$$

Method 2: Given an interpolatory FIR filter, the construction of its dual filters is provided in a number of papers [7, 12]. In this paper, we extend the work of [7] from FIR to IIR.

Proposition 2. *Let M_0 be a lowpass filter satisfying Eq. (2). Then, for each $J\in\mathbb{Z}^+$ the filter,*

$$M_0^d=\binom{2J}{J}M_0^J(1-M_0)^J+\sum_{j=0}^{J-1}\binom{2J}{j}M_0^{2J-1-j}(1-M_0)^j \tag{6}$$

is a dual filter of M_0 with $M_0^d(0)=1$.

Proof: Using Eq. (2) and $\binom{2J}{j}=\binom{2J}{2J-j}$, we have

$$\begin{aligned}M_0^d(\xi+\frac{1}{2}) &= \binom{2J}{J}M_0^J(\xi+\frac{1}{2})[1-M_0(\xi+\frac{1}{2})]^J\\ &\quad+\sum_{j=0}^{J-1}\binom{2J}{j}M_0^{2J-1-j}(\xi+\frac{1}{2})[1-M_0(\xi+\frac{1}{2})]^j\\ &= \binom{2J}{J}M_0^J(\xi)[1-M_0(\xi)]^J\\ &\quad+\sum_{j=0}^{J-1}\binom{2J}{2J-j}[1-M_0(\xi)]^{2J-1-j}M_0^j(\xi)\end{aligned}$$

Hence,

$$M_0(\xi)\overline{M_0^d(\xi)}+M_0(\xi+\frac{1}{2})\overline{M_0^d(\xi+\frac{1}{2})}=[M_0(\xi)+(1-M_0(\xi))]^{2J}=1. \tag{7}$$

Finally, since $M_0(0)=1$, using the definition of M_0^d, we conclude that $M_0^d(0)=1$. □

Let M_0^d be given by Eq. (6). Then, the dual filter M_0^d satisfies $M_0^d(\xi)=1+O(|\xi|)$. Since the infinite product $\widehat{\Phi}^d(\xi)=\prod_{k=1}^{\infty}M_0^d(\frac{\xi}{2^k})$ converges uniformly on any compact set, it is continuous. This implies that $\widehat{\Phi}^d$ is well defined. Therefore, if the function Φ^d is in $L^2(\mathbb{R})$ and Φ^d and its shifts form a Riesz basis, then Φ^d will be a dual scaling function for Φ.

In summary, using Method 1 we can directly construct a stable dual scaling function Φ^d of the scaling function Φ. Using Method 2, we can easily get a dual filter M_0^d for M_0. Eq. 7 establishes that these two filters induce a perfect reconstruction filter bank. What remains to be checked is whether the function Φ^d is in

$L^2(\mathbb{R})$ and Φ^d and its integer shifts form a stable set. In our work, we used Method 2 to obtain the dual filter M_0^d of M_0 with $J = 1$, i.e., $M_0^d = M_0(\xi)[3 - 2M_0(\xi)]$. The main reason being that for any N, the maximum values of the filters M_0^d obtained from Eq. (5) and Eq. (6) are $\frac{1}{2}(1 + \sqrt{2})$ and 1.125, respectively. These values are achieved at the same point $\xi_0 \in [0, \frac{1}{2}]$ with $M_0(\xi_0) = \frac{3}{4}$.

Let's assume that M_0^d obtained by Method 2. It is not difficult to show that 1) M_0 and M_0^d are C^1 functions at the points $k \pm \frac{1}{4}$ for all $k \in \mathbb{Z}$, 2) at the points $k \pm \frac{1}{2}$, M_0 and M_0^d are C^∞ functions for odd N and C^N functions for even N; and 3) the resulting biorthogonal wavelets have $2N + 2$ vanishing moments.

2.2 g-HDAF Multiresolution Deformable Models for Shape Modeling

The models used in this work are three-dimensional surface shape models. The material coordinates $\mathbf{u} = (u, v)$ of a point on these models are specified over a domain Ω [11, 13]. The position of a point (with material coordinates $\mathbf{u}$) on a deformable model at time t with respect to an inertial reference frame Φ is given by: ${}^{\Phi}\mathbf{x}(\mathbf{u}, t) = {}^{\Phi}\mathbf{t}(t) + {}^{\Phi}_{\phi}\mathbf{R}(t)\ {}^{\phi}\mathbf{p}(\mathbf{u}, t)$, where ${}^{\Phi}\mathbf{t}$ is the position of the origin O of the model frame ϕ with respect to the frame Φ (the model's translation), and ${}^{\Phi}_{\phi}\mathbf{R}$ is the matrix that determines the orientation of ϕ with respect to Φ. ${}^{\phi}\mathbf{p}(\mathbf{u}, t)$ denotes the position of a model point with material coordinates $\mathbf{u}$ w.r.t. the model frame. It can be expressed as the sum of a reference shape ${}^{\phi}\mathbf{s}(\mathbf{u}, t)$ and a local displacement ${}^{\phi}\mathbf{d}(\mathbf{u}, t)$: ${}^{\phi}\mathbf{p}(\mathbf{u}, t) = {}^{\phi}\mathbf{s}(\mathbf{u}, t) + {}^{\phi}\mathbf{d}(\mathbf{u}, t)$. The reference shape, $\mathbf{s}$, captures the salient shape features of the model and it is the result of applying global deformations, $\mathbf{T}$, to a geometric primitive $\mathbf{e} = [e_x, e_y, e_z]^\top$. The geometric primitive $\mathbf{e}$ is defined parametrically in $\mathbf{u} \in \Omega$ and has global shape parameters $\mathbf{q_e}$. For the purposes of this research, we employ a superquadric $\mathbf{e}(u, v)[-\frac{\pi}{2}, \frac{\pi}{2}) \times [-\pi, \pi) \rightarrow \mathbb{R}^3$, whose global shape parameters are $\mathbf{q_e} = [a_1, a_2, a_3, \epsilon_1, \epsilon_2]^\top$. A superquadric surface is defined by a vector sweeping a closed surface in space by varying the material coordinates u and v. The parametric equation of a superquadric is given by [1]:

$$\mathbf{e}(\mathbf{u}) = [a_1 {C_u}^{\epsilon_1} {C_v}^{\epsilon_2}, a_2 {C_u}^{\epsilon_1} {S_v}^{\epsilon_2}, a_3 {S_u}^{\epsilon_1}]^\top,$$

where $-\frac{\pi}{2} \leq u \leq \frac{\pi}{2}$, $-\pi \leq v \leq \pi$, $S_u = \text{sgn}(\sin\ u)|\sin\ u|^\epsilon$, $C_u = \text{sgn}(\cos\ u)|\cos\ u|^\epsilon$, and $a_1, a_2, a_3 \geq 0$ are the parameters that define the superquadric size, and ϵ_1 and ϵ_2 are the "squareness" parameters in the latitudinal and longitudinal planes, respectively. Local displacements $\mathbf{d}$ are computed using finite elements. Associated with every finite element node i is a nodal vector variable $\mathbf{q}_{d,i}$. We collect all the nodal variables into a vector of local degrees of freedom $\mathbf{q}_d = (\ldots, \mathbf{q}_{d,i}^\top, \ldots)^\top$. If we denote the original nodal discretization at resolution $j = 0$ by the vector α_0, then $\alpha_0 = \mathbf{H}^d\mathbf{q}_d$ (analysis) and $\mathbf{q}_d = \mathbf{H}\alpha_0$ (reconstruction), where the matrices $\mathbf{H}$ and $\mathbf{H}^d$ correspond to the g-HDAFs and the vector $\mathbf{q}_{d,i}$ is hierarchically expressed with respect to the new biorthonormal basis. We compute the local displacement $\mathbf{d}$ based on the finite element theory as $\mathbf{d}(u, v) = \mathbf{S}\mathbf{q}_d(u, v)$. Here, $\mathbf{S}$ is the shape matrix whose entries are the finite element shape functions.

2.3 Surface Fitting

Through the application of Lagrangian mechanics, the geometric parameters of the deformable model, the global (parameterized) and the local (free-form) deformation parameters, and the six degrees of freedom of rigid-body motion are systematically converted into generalized coordinates or dynamic degrees of freedom as described in [11]. The resulting Lagrangian equations are of the form $\dot{\mathbf{q}} + \mathbf{K}\mathbf{q} = \mathbf{f}_q$, for shape estimation, where $\mathbf{K}$ is the stiffness matrix, the $\mathbf{f}_q$ are the generalized external forces that act on the model, and the $\mathbf{q}$ are the model's generalized coordinates. The damping and the stiffness matrices determine the viscoelastic properties of the deformable model. Expressing the stiffness matrix in the g-HDAF wavelet basis is explained in detail in [8]. In physics-based shape estimation techniques, data points apply forces to the deformable model. These forces are converted to generalized 3D forces. Based on these forces the model will deform to minimize the discrepancy between the model and the data.

3 Experimental Results

We have applied the new multiresolution shape models for recovering the 3D surface shape from synthetic and real range data. We have assessed the accuracy, limitations, and advantages of the g-HDAF deformable models by comparing the performance of the multiresolution deformable models constructed using g-HDAFs (Gn), m-HDAFs (Hn), Daubechies (Dn), Symlets (Sn) [2], the Butterworth filter (Bn) [3], the orthogonal spline filter (M) [10], the orthogonal fractional splines (Fn) [14] with X vanishing moments, Coiflets (Cn) with 2X vanishing moments, and the orthogonal spline with 4 vanishing moments. Due to space restrictions, we present only selected results. Complete results for a variety of data and the complete set of the wavelet bases we examined can be found at [8].

In the first experiment, we applied our technique to fit synthetic data obtained from a graphical model of a chess piece. Fig. 1(a) depicts the data, Fig. 1(b) depicts the estimated shape model, while Figs. 1(c-e) depict the estimated (by the fitting process) displacement maps $\mathbf{q}_{d_x}(u,v)$, $\mathbf{q}_{d_y}(u,v)$ and $\mathbf{q}_{d_z}(u,v)$, respectively. In the second experiment, we applied our technique to fit female breast surface data. Fig. 1(f) depicts the breast range data obtained from a subject, Fig. 1(g) depicts the estimated shape model, while Figs. 1(h-j) depict the estimated displacement maps $\mathbf{q}_{d_x}$, $\mathbf{q}_{d_y}$ and $\mathbf{q}_{d_z}$, respectively.

Table 1 shows the RMSE of the reconstructed maps using the LL subband only. To evaluate the efficiency of the g-HDAF filter, Table 2 shows the RMSE performance (R) for a sequence of the estimated displacement maps if all high-pass subbands are suppressed. The corresponding results for various filters are also included. Table 3 contains the number of transform coefficients of one level decomposition that can be ignored if we require the RMSE of the reconstructed $\mathbf{q}_{d_x}(u,v)$, $\mathbf{q}_{d_y}(u,v)$ and $\mathbf{q}_{d_z}(u,v)$ to be 0.0001. Applying this procedure to a sequence of the estimated displacement maps, Table 4 depicts the percentage of the insignificant coefficients when the RMSE of the reconstructed maps is 0.0001. Again, for comparison, other filters are included in this table. From above four tables, we can see that the g-HDAF filters perform best among all the filters exam-

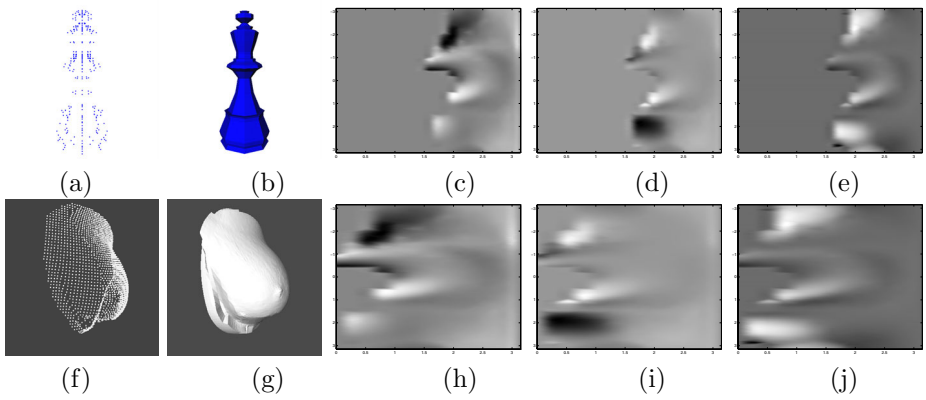

Figure 1: (a,f) Synthetic data from a graphics model of a chess piece and real range data from a female patient's breast. (b,g) The estimated deformable models, and (c-e,h-j) depiction of $\mathbf{q}_{d_x}(u,v)$, $\mathbf{q}_{d_y}(u.v)$ and $\mathbf{q}_{d_z}(u,v)$, respectively.

ined in this paper. Since our filters are symmetric, we use the symmetric extension of the functions $\mathbf{q}_{d_x}$, $\mathbf{q}_{d_y}$ and $\mathbf{q}_{d_z}$, and the most favorable extension for the other families.

The main reasons for obtaining an overall improved performance using the proposed filters are the following. First, all g-HDAF biorthonormal wavelets are literally linear phase wavelets. The linear phase, which is the result of symmetry of the corresponding low pass filters, enhances the sparsity of wavelet decompositions, especially if the input matrix is symmetrically padded. Second, g-HDAFs appear to be smoother than their Daubechies / Symlets / Coiflets counterparts with the same number of vanishing moments. In addition, the symmetry of the low pass filters reduces the computational complexity. However, one possible drawback could be the significant length of g-HDAF filters (in this paper, we used filters with 23 filter taps for M_0 and 45 taps for M_0^d). Although, g-HDAFs have infinite length only a small portion of their filter taps, located around the origin, plays the significant role in the wavelet transform. This is due to the good localization of the g-HDAF scaling functions and wavelets in the time domain, which, in turn, is due to the optimal localization of the HDAFs in the time domain. Note, also, that the length of the significant part of the low pass filters remains almost the same for any number of vanishing moments.

4 Concluding Remarks

In this paper, we presented the construction of a new class of linear phase wavelets (g-HDAFs) and the development of a new class of deformable models using this new biorthogonal wavelet basis. Experimental results indicate that the g-HDAF multiresolution deformable models achieve higher energy compaction than those based on conventional wavelets. This attribute makes them useful for shape reconstruction, shape recognition, and geometry compression.

Table 1: The estimated (by the fitting process) displacement maps $\mathbf{q}_{d_x}$, $\mathbf{q}_{d_y}$, $\mathbf{q}_{d_z}$ are decomposed one level by interpolating g-HDAF filters (Gn) and m-HDAF filters (Hn). The table shows the RMSE (R) of the reconstructed maps if all the detail subbands are suppressed.

	$\mathbf{q}_{d_x}$	$\mathbf{q}_{d_y}$	$\mathbf{q}_{d_z}$		$\mathbf{q}_{d_x}$	$\mathbf{q}_{d_y}$	$\mathbf{q}_{d_z}$
W	R	R	R	W	R	R	R
G2	1.1625	1.3390	2.5604	H2	1.5623	1.8138	3.3715
G3	1.1118	1.2789	2.4434	H3	1.3706	1.5867	2.9955
G4	1.0826	1.2440	2.3740	H4	1.2737	1.4732	2.7961
G5	1.0631	1.2205	2.3269	H5	1.2160	1.4055	2.6732
G6	1.0489	1.2033	2.2922	H6	1.1776	1.3602	2.5894
G7	1.0380	1.1900	2.2653	H7	1.1501	1.3276	2.5281
G8	1.0292	1.1794	2.2436	H8	1.1293	1.3028	2.4809
G9	1.0220	1.1705	2.2257	H9	1.1128	1.2831	2.4432
G10	1.0158	1.1631	2.2104	H10	1.0995	1.2671	2.4122
G11	1.0106	1.1566	2.1973	H11	1.0884	1.2537	2.3861
G12	1.0060	1.1510	2.1858	H12	1.0789	1.2423	2.3639
G13	1.0019	1.1461	2.1757	H13	1.0708	1.2324	2.3445
G14	0.9982	1.1417	2.1666	H14	1.0636	1.2238	2.3275
G15	0.9949	1.1377	2.1585	H15	1.0574	1.2161	2.3124

Table 2: The estimated (by the fitting process) displacement maps obtained from the proposed deformation model are decomposed one level by g-HDAF filters (Gn), Daubechies' orthogonal filter (Dn), least symmetric orthogonal filters (Sn), Coiflets (Cn), the orthogonal spline filter (M), the Butterworth filters (Bn), and the fractional spline filters (Fn). Depicted are the mean and variance of the reconstructed maps if all the detail subbands are suppressed.

W	(Mean,Var.)	W	(Mean,Var.)	W	(Mean,Var.)	W	(Mean,Var.)
G2	(0.0019, 0.0036)	H2	(0.0030,0.0059)	D4	(0.0042,0.0078)	C4	(0.0032,0.0058)
G4	(0.0017, 0.0033)	H4	(0.0021,0.0041)	D8	(0.0030,0.0055)	M	(0.0017,0.0032)
G6	(0.0017, 0.0032)	H6	(0.0019,0.0037)	D12	(0.0034,0.0064)	B5	(0.0035,0.0065)
G8	(0.0017, 0.0032)	H8	(0.0018,0.0035)	S4	(0.0034,0.0062)	B9	(0.0033,0.0061)
G10	(0.0016 0.0031)	H10	(0.0017,0.0034)	S8	(0.0031,0.0056)	B13	(0.0032,0.0059)
G12	(0.0016 0.0031)	H12	(0.0017,0.0033)	S12	(0.0031,0.0058)	F4	(0.0033,0.0062)
G14	(0.0016 0.0031)	H14	(0.0017,0.0032)	S14	(0.0031,0.0058)	F12	(0.0032,0.0059)

Table 3: The estimated (by the fitting process) displacement maps $\mathbf{q}_{d_x}$, $\mathbf{q}_{d_y}$, $\mathbf{q}_{d_z}$ are decomposed one level by interpolating g-HDAF filters (Gn). The table shows how many coefficients can be ignored if the RMSE of the reconstructed maps is 0.0001.

	$\mathbf{q}_{d_x}$	$\mathbf{q}_{d_y}$	$\mathbf{q}_{d_z}$		$\mathbf{q}_{d_x}$	$\mathbf{q}_{d_y}$	$\mathbf{q}_{d_z}$		$\mathbf{q}_{d_x}$	$\mathbf{q}_{d_y}$	$\mathbf{q}_{d_z}$
W	LS	LS	LS	W	LS	LS	LS	W	LS	LS	LS
G2	201988	201156	203212	H2	201504	200480	202912	D8	201568	200800	203424
G4	202012	201196	203180	H4	201824	200928	203360	S4	201632	200672	203360
G6	202012	201212	203140	H6	201888	200992	203424	S8	201568	200800	203424
G8	202020	201220	203116	H8	201888	201056	203360	C4	201696	200864	203360
G10	202020	201220	203100	H10	201888	201056	203360	M	201952	201120	203296
G12	202020	201228	203084	H12	201952	201120	203296	B9	204000	204128	208288
G14	202020	201228	203076	H14	201952	201120	203296	F8	204896	204704	208544

Table 4: The estimated (by the fitting process) displacement maps obtained from the proposed deformation model are decomposed one level. The table shows how many coefficients (on average) can be ignored if the RMSE of the reconstructed maps is 0.0001.

W	(Mean,Var.)	W	(Mean,Var.)	W	(Mean,Var.)	W	(Mean,Var.)
G2	(0.8083 0.0536)	H2	(0.8035,0.0523)	D4	(0.7050,0.2107)	C4	(0.7066,0.2088)
G4	(0.8083 0.0537)	H4	(0.8050,0.0519)	D8	(0.7072,0.2071)	M	(0.8052,0.0520)
G6	(0.8083 0.0537)	H6	(0.8051,0.0519)	D12	(0.7008,0.2169)	B5	(0.7594,0.1370)
G8	(0.8083 0.0537)	H8	(0.8052,0.0520)	S4	(0.7058,0.2099)	B9	(0.7536,0.1460)
G10	(0.8083 0.0537)	H10	(0.8052,0.0520)	S8	(0.7057,0.2104)	B13	(0.7512,0.1495)
G12	(0.8083 0.0537)	H12	(0.8052,0.0520)	S12	(0.7150,0.1903)	F4	(0.7622,0.1316)
G14	(0.8082 0.0537)	H14	(0.8052,0.0520)	S14	(0.7143,0.1918)	F12	(0.7540,0.1462)

References

[1] A. Barr. Global and local deformations of solid primitives. *Computer Graphics*, 18(3):21–30, 1984.

[2] I. Daubechies. *Ten Lectures on Wavelets*. SIAM, 1992.

[3] C. Herley and M. Vetterli. Wavelets and recursive filter banks. *IEEE Transactions on Signal Processing*, 41(8):2536–2556, 1993.

[4] D. Hoffman and D. Kouri. Distributed approximating functional theory for an arbitrary number of particles in a coordinate system independent formalism. *Journal of Physical Chemistry*, 97:4984–4988, 1993.

[5] D. Hoffman, N. Nayar, O. A. Sharafeddin, and D. Kouri. On an analytic banded approximation for the discretized free propagator. *Journal of Physical Chemistry*, 95:8299, 1991.

[6] D. Hoffman, G. W. Wei, D. S. Zhang, and D. Kouri. Shannon-Gabor wavelet distributed approximating functional. *Chemical Physics Letters*, 287:119–124, 1998.

[7] H. Ji and Z. Shen. Compactly supported (bi)orthogonal wavelets generated by interpolatory refinable functions. *Advances in Computational Mathematics*, pages 81–104, 1999.

[8] I. Kakadiaris, M. Papadakis, L. Shen, D. Kouri, and D. Hoffman. m-HDAF multiresolution deformable models. Technical Report 02-70, Department of Computer Science, University of Houston, Houston, TX, February 2002.

[9] S. Mallat. Multiresolution approximations and wavelet orthonormal bases of $L^2(R)$. *Trans. Amer. Math. Soc.*, 315:69–87, 1989.

[10] S. G. Mallat. A theory for multi-resolution signal decomposition: The wavelet representation. *IEEE Trans. Pattern Analysis and Machine Intelligence*, 11(7):674–693, 1989.

[11] D. Metaxas and D. Terzopoulos. Shape and nonrigid motion estimation through physics-based synthesis. *IEEE Transactions on Pattern Analysis and Machine Intelligence*, 15(6):580 – 591, June 1993.

[12] W. Swelden. The lifting scheme: A custom-designed construction of biorthogonal wavelets. *Applied and Computational Harmonic Analysis*, 3:186–200, 1996.

[13] D. Terzopoulos and D. Metaxas. Dynamic 3D models with local and global deformations: Deformable superquadrics. *IEEE Transactions on Pattern Analysis and Machine Intelligence*, 13(7):703 – 714, 1991.

[14] M. Unser and T. Blu. Fractional splines and wavelets. *SIAM Review*, 42(1):43–67, March 2000.

[15] B. Vemuri and A. Radisavljevic. Multiresolution stochastic hybrid shape models with fractal priors. *ACM Transactions on Graphics*, 13(2):177–207, April 1994. Special Issue on Interactive Sculpting.